ACS OMEGA

Article

Cite This: ACS Omega 2019, 4, 14211−14218

http://pubs.acs.org/journal/acsodf

Mechanistic Understanding of the Phosphorylation-Induced Conformational Rigidity at the AMPA Receptor C-terminal Domain

Sudeshna Chatterjee,[†] Chayan Dutta,[†] Nicole C. Carrejo,[†] and Christy F. Landes*[,†,‡]

[†]Department of Chemistry and [‡]Department of Electrical and Computer Engineering, Rice University, Houston, Texas 77005, United States

Supporting Information

ABSTRACT: Phosphorylation at the intracellular C-terminal domain (CTD) of α-amino-3-hydroxy-5-methyl-4-isoxazolepropionic acid (AMPA) receptors induces conformational rigidity. Such intracellular alterations to the AMPA receptor influence its functional responses, which are involved in multiple synaptic processes and neuronal signaling. The structure of the CTD still remains unresolved, which poses challenges toward providing a mechanism for the process of phosphorylation and deciphering the role of each phosphorylation step in causing the resultant conformational behavior. Herein, we utilize smFRET spectroscopy to understand the mechanism of phosphorylation, with the help of strategic point mutations that mimic phosphorylation. Our results reveal that first, phosphorylation at three target sites (S818, S831, and T840) is necessary for the change in the secondary structure of the existing disordered native sequence. Also, the results suggest that the formation of the tertiary structure through electrostatic interaction involving one specific phosphorylation site (S831) stabilizes the structure and renders conformational rigidity.

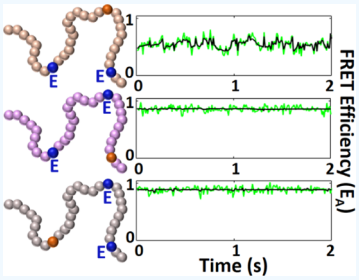

INTRODUCTION

α-Amino-3-hydroxy-5-methyl-4-isoxazolepropionic acid (AMPA) receptors are a class of ionotropic glutamate receptors that mediate excitatory synaptic signals across neuronal membranes.[1−5] Neuronal transmission through AMPA receptor ion channels is responsible for the development of memory and other cognitive functions.[6−10] AMPA receptors undergo several extra and intracellular modifications, which in turn modulate its functionality.[6,11−14] Therefore, unraveling the mechanism of such modifications is of enormous significance for the determination of appropriate drug targets for several neurological treatments.[15−18]

Intracellular modifications at the C-terminal domain (CTD) of AMPA receptors are crucial to several synaptic processes such as long-term potentiation,[6,7,9−11,14] but a detailed structural description of the CTD is not yet available. X-ray crystallography succeeds in resolving the structure of all of the other domains of AMPA receptors, barring the CTD, due to its inherent flexibility.[19] Functional responses to the intracellular modifications, such as phosphorylation, palmitoylation, etc., have been successfully demonstrated with electrophysiological measurements.[12,20−22] However, a detailed mechanism involving conformational changes of the receptors, and their heterogeneous dynamics is yet to be explored.

Previous studies have shown that Ca^{2+}-mediated phosphorylation at S818, S831, and T840 enhances the conductance of ions through the AMPA receptor channel and is crucial to long-term potentiation.[13,20−22] Furthermore, our previous study on a membrane proximal section of the CTD showed that mutating the aforementioned three phosphorylation sites with phosphorylation mimicking Glu residues introduces conformational rigidity to the structure.[23] In addition, these studies demonstrated that such conformational changes were electrostatically tunable, suggesting a mechanism that involves electrostatic interaction. However, the mode of such electrostatic interaction and contribution of each specific mutation toward conformational rigidity remain to be explained.

Other work demonstrated that phosphorylation at different sites can have nonidentical functional responses, for example, S831 phosphorylation directly enhances the function of the AMPA receptor by enhancing the channel conductance.[20,22,24,25] In contrast, S818 phosphorylation facilitates the synaptic incorporation of AMPA.[12,14] Thus, resolving the effects of each phosphorylation toward the overall structural changes of the CTD of the AMPA receptor is necessary. We speculate that the phosphomimetic mutations at S818, S831, and T840 change the secondary structure of the native sequence, and the structure is further stabilized through the formation of the salt bridge between the negatively charged Glu residues and nearby positively charged residues.[23] In this study, we implemented a stepwise mutation strategy that successfully indicated which phosphorylation site(s) play(s) major role in the formation of a stable tertiary structure possibly through the formation of the salt bridge.

Herein, we used single-molecule Förster resonance energy transfer (smFRET) spectroscopy to probe the conformational changes of three different mutant variations of a 34 amino acid section of the CTD, reported in our previous study.[23] smFRET

Received: May 13, 2019
Accepted: August 6, 2019
Published: August 20, 2019

is a popular technique that has been extensively applied to resolve the complex dynamics of biomolecules.[26−33] By utilizing smFRET spectroscopy, we probed the conformational dynamics explored by the three mutant variations. The results revealed that phosphomimetic mutation at S831 is necessary for the electrostatic interaction, which stabilizes the secondary structure of the CTD, thereby rendering the conformational rigidity.

RESULTS AND DISCUSSION

Phosphomimetic Mutations are Turned Off Sequentially to Determine the Role of Each Mutation in Rendering Conformational Rigidity. Figure 1A shows the modeled full-length structure of the AMPA receptor, along with the primary sequences of the native 34 amino acid section and the same section with the three phosphomimetic mutations (E10E23E32). In the E10E23E32 peptide, E10, E23, and E32 mutations mimic the phosphorylation at S818, S831, and T840 residues of the AMPA receptor CTD, respectively. It has been demonstrated previously that the formation of the salt bridge is feasible between oppositely charged amino acid residues that can result in a stable tertiary structure.[32,34−38] In the case of the E10E23E32 peptide, there are positively charged arginine (R7, R12, R29) and lysine (K5, K14) residues in the vicinity of the negatively charged phosphomimetic Glu residues that can facilitate such formations of the salt bridge. It is necessary to understand exactly which phosphomimetic residue(s) can potentially contribute to such formation, for two reasons. First, it will support the proposed mechanism that the rigidity is a result of a change in the secondary structure, followed by a tertiary stabilization. Second, it will provide a deeper understanding of stepwise phosphorylation and will resolve the functional responses of phosphorylation at each target. Therefore, three different peptide constructs are chosen. On each construct, one of the mutations is turned off by leaving the native amino acid unmutated. Figure 1B depicts the primary sequences of the resulting mutants, E10S23E32 (E23 mutation is off), E10E23T32 (E32 mutation is off), and S10E23E32 (E10 mutation is off). All of the peptide constructs have a Biotin tag at the N-terminal end to accommodate immobilization single molecules. Furthermore, they are labeled with a FRET compatible pair of donor (Alexa 555) and acceptor (Alexa 647) fluorophores at C3 and C34 for enabling the acquisition of smFRET. Changes in the conformational behavior in the absence of each of the three mutations are monitored with smFRET.

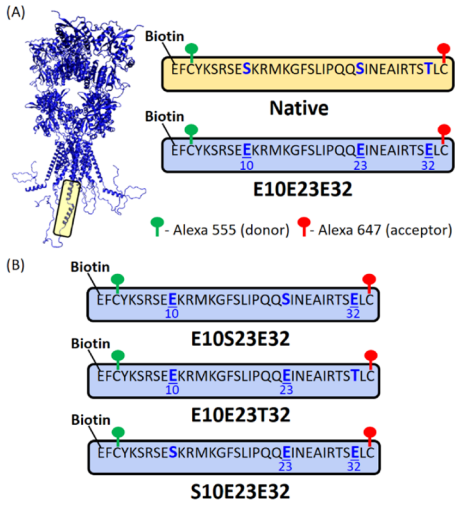

Figure 1. Primary sequences of the peptides being studied with their corresponding glutamic acid mutations. (A) Modeled structure of full AMPA receptor, based on the homology model reported by Jenkins et al.[21] Jenkins et al. used the sequences of GluA1 and GluA2 and the crystal structure of *Rattus norvegicus* GluA2 (PDB ID: 3KG2) in their modeling. The squared section shows the 34 amino acid long section of the CTD under the study. The corresponding primary sequence is shown in the yellow box labeled as "Native". Phosphomimetic glutamic acid mutations are introduced at 10, 23, and 32, shown in the blue box labeled as "E10E23E32". (B) Primary sequences of the mutants are depicted, where one of the three phosphomimetic mutations is switched off in each, to test the role of each site in introducing the conformational rigidity. The model structure in panel (A) has been recreated in part from ref 21. Copyright 2014 American Society for Pharmacology and Experimental Therapeutics (ASPET).

E23 Mutation (Mimicking S831 Phosphorylation) is Necessary for Establishing Conformational Rigidity through Electrostatic Interaction. Denoised smFRET efficiency trajectories are histogrammed for each peptide. The numbers of single-molecule trajectories analyzed for each mutant and condition are included in the Supporting Information. Figure 2A compares distributions of the smFRET efficiency of the three mutants with those of the previously reported[23] native (blue) and E10E23E32 peptide (dark green). The E10S23E32 peptide (light brown) explores a broad range of FRET efficiencies similar to that explored by the native peptide and is in contrast to the narrower distribution explored by the E10E23E32 peptide. On the other hand, the E10E23T32 peptide (purple) and the S10E23E32 peptide (dark brown) explore a narrower range of conformations, resembling that of the E10E23E32 peptide. All of the five peptides exhibit >50% population in the high FRET efficiency range of 0.80−1.00, indicated by the peaks appearing at 0.96 (native), 0.98 (E10E23E32), 0.88 (E10S23E32), 0.88 (E10E23T32), and 0.92 (S10E23E32). However, similar to the native peptide, the E10S23E32 peptide explores several other conformations corresponding to the intermediate and low FRET efficiencies, ranging between 0.40 and 0.78. In contrast, the E10E23T32, the S10E23E32 peptide, and the E10E23E32 peptide primarily remain in the FRET efficiency range of 0.80−1.00. Table S1 in the Supporting Information shows the differences in populations of each peptide distributed among region A (0.80−1.00) and region B (0.40−0.78). Thus, the distributions of smFRET efficiency show that the absence of the E23 mutation allows the peptide to explore a broad range of conformations, similar to the native peptide. It should be noted here that the distance between the probes can increase beyond the FRET detection range, especially given the dynamic nature of the mutants. However, all of the mutants are studied under the same experimental conditions, and their dynamics are probed within the same standard FRET efficiency detection region. Hence, the variation of FRET efficiency for different mutants represents real dynamic conformational behavior for these disordered structures. Furthermore, our previous results with full-length NMDA receptor has shown that higher apparent FRET efficiency (E_A) values do correspond to real distances obtained from crystallography data.[39] Thus, we think that even our high E_A values correspond to real conformational behavior and not just the absence of the molecule in the sensitive FRET range.

DOI: 10.1021/acsomega.9b01384
ACS Omega 2019, 4, 14211−14218

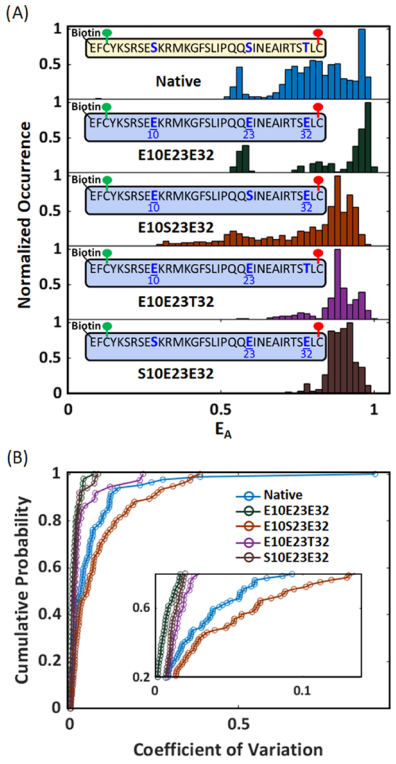

Figure 2. Phosphomimetic E23 mutation is necessary for conformational rigidity. (A) smFRET efficiency (E_A) distributions of the native peptide (blue), the E10E23E32 peptide (dark green), the E10S23E32 peptide (light brown), the E10E23T32 peptide (purple), and the S10E23E32 peptide (dark brown), under the standard buffer (1×) condition, are depicted along with the corresponding primary sequences. (B) Cumulative probability distributions of the CV of the single-molecule trajectories are plotted for all five peptides. Inset: zoomed-in on a section of the plot. Note that a faster CV decay indicates a more rigid peptide, whereas a slower decay indicates a more flexible peptide. The numbers of single-peptide trajectories analyzed are 84, 49, 76, 37, and 50 for the native, E10E23E32, E10S23E32, E10E23T32, and S10E23E32 peptides, respectively.

Figure S1 in the Supporting Information presents sample trajectories and histograms for a portion of the NMDA receptor protein having a well-defined structure measured using the same experimental setup.[39] This result shows that the trajectories and histograms presented here reflect dynamics in CTD mutant conformations. Moreover, the CTD does not exhibit a well-defined structure in the protein crystallographic analysis, whereas all other domains of this family of proteins are well defined.[19,40] Thus, the dynamic nature and lack of a defined conformation exhibited by the CTD peptides are consistent with previous protein crystallography studies[19] and computational structure predictions.[23]

The conformational flexibility or rigidity exhibited by the peptides is quantified and compared using the coefficient of variation (CV) analysis. As reported in our previous work,[23] state assignment using vbFRET[41] failed to provide a reasonable solution to the smFRET data obtained from the native and the E10E23E32 peptide. Similarly, vbFRET suggests best fits at 21, 14, and 10 states for the E10S23E32, E10E23T32, and S10E23E32 peptides, respectively (Figure S2). This result supports the dynamic nature exhibited by not only the native peptide but by the phosphomimetic mutants as well. Furthermore, we utilized 3D structure prediction algorithms, PEP-FOLD[42] and Bhageerath,[43] to obtain structural information for the native and the E10E23E32 peptides in our previous work.[23] These algorithms did not converge to one or a few most probable conformation(s) but rather predicted multiple distinct conformations.[23] Hence, CV analysis has been employed to quantify the conformational fluctuations exhibited by the peptides. The CV of each smFRET trajectory is calculated, and the cumulative probabilities for the CV of all trajectories are plotted in Figure 2B. A steeper decay in CV corresponds to fewer overall variations of smFRET efficiencies and, therefore, a more rigid conformation. Conversely, a slower decay of CV indicates higher conformational variability of the peptide. The decays of the CV plots corresponding to the native and the E10E23E32 peptide set two extremes for the conformational variability, with the native peptide (blue) exhibiting more conformational flexibility and the E10E23E32 peptide (light brown) exhibiting less. As the E23 mutation is present in both the E10E23T32 peptide (purple) and the S10E23E32 peptide (dark brown), the peptides tend to be conformationally rigid, almost resembling the E10E23E32 peptide. However, when the E23 mutation is absent, the E10S23E32 peptide (light brown) shows even higher flexibility than the native peptide. This behavior agrees with the observation that the E10S23E32 peptide explores a broader range of smFRET efficiencies than the native peptide (Figure 2A).

Further quantification by the standard deviation (SD) analysis supports the conclusion that the E23 mutation causes a narrower range of conformations to be explored as compared to the native sequence. The SD of each single-molecule trajectory is calculated, and SD distributions incorporating all of the trajectories are plotted in Figure S3, for each peptide. The width of the SD distributions and the SD values directly imply the variations of conformations explored by the peptides. Figures 2A, B and S3 demonstrate that the presence of the E23 mutation, with either of the other two mutations, causes fewer conformations being explored, indicating a rigid structure, as opposed to the flexible nature exhibited by the native and the E10S23E32 peptide. Our results suggest that the E23 mutation is necessary for the conformational rigidity of the structure, irrespective of the presence of either of the E10 and the E32 mutations.

Variation of the Salt Concentration Confirms that the Rigidity Caused by the E23 Mutation is Electrostatically Tunable. In our previous work, we showed that the conformational rigidity of the E10E23E32 peptide-induced multiple phosphomimetic mutations is electrostatically tunable.[23] At a high ionic strength, the charges introduced by the Glu mutations are shielded, and hence their contribution toward the conformational rigidity are minimized, rendering flexibility similar to the native peptide.[23] Herein, we have implemented the same strategy to verify if the E23 mutation specifically is electrostatically tunable. This strategy will verify if the formation of a tertiary electrostatic is taking place through the E23 mutation, causing rigidity. In Figure 3, panels A, B, and C show the primary sequences of the peptides (top), the corresponding distribution of smFRET at increasing salt concentrations (middle), and the CV analyses (bottom) of the smFRET data, for the E10E23E32, E10E23T32, and S10E23E32 peptides respectively. 1× represents the buffer solution containing 137 mM NaCl and 2.7 mM KCl. 2× and 5× represent buffer solutions containing two and five times as much the NaCl and KCl concentrations as in 1×. The

DOI: 10.1021/acsomega.9b01384
ACS Omega 2019, 4, 14211−14218

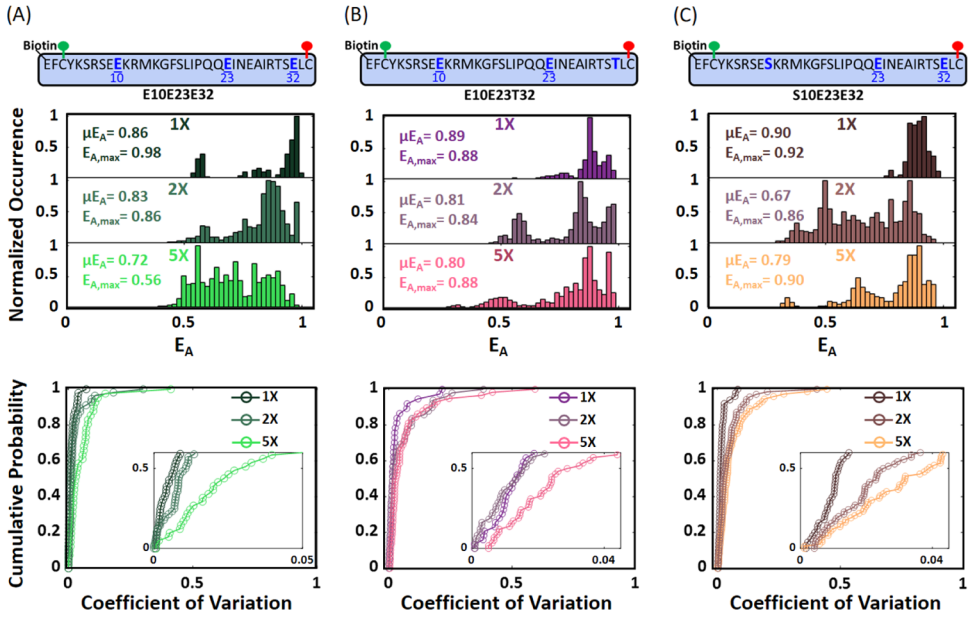

Figure 3. E23 is the primary contributor to electrostatic tunability of conformational rigidity. (A) Primary sequence (top), distributions of smFRET efficiency (E_A) under varying salt concentrations (middle), and CV analysis (bottom) for the E10E23E32 peptide. (B) Primary sequence (top), distributions of smFRET efficiency under varying salt concentrations (middle), and CV analysis (bottom) for the E10E23T32 peptide. (C) Primary sequence (top), distributions of smFRET efficiency under varying salt concentrations (middle), and CV analysis (bottom) for the S10E23E32 peptide. The salt concentrations are varied as 1× ([NaCl] = 137 mM, [KCl] = 2.7 mM), 2× ([NaCl] = 274 mM, [KCl] = 5.4 mM), and 5× ([NaCl] = 685 mM, [KCl] = 13.5 mM). μE_A and $E_{A,max}$ represent mean and most probable smFRET efficiencies, respectively. The number of molecules included in the analysis for each condition is mentioned in the Supporting Information.

E10E23E32 peptide loses its conformational rigidity as the salt concentration is increased and gains flexibility similar to the native peptide. The E10E23T32 peptide and the S10E23E32 peptide also exhibit similar electrostatic tunability. At increasing salt concentrations, distributions of smFRET of both the peptides become broader, and the cumulative probabilities of CV show increasingly slower decay. Thus, it is confirmed that shielding of the charge of E23 weakens the electrostatic formation, thereby reducing the rigidity and making the peptide flexible similar to the native peptide.

The native peptide retains its flexibility even at high salt concentrations as demonstrated in Figure S4, as this inherent flexibility is not a result of electrostatic interactions. Similarly, the E10S23E32 peptide does not lose its flexibility at a high salt concentration. It is to be noted that unlike the native peptide, the E10S23E32 peptide does have two negative charges at the E10 and E32 mutations. Yet, shielding those charges does not affect its flexibility, thereby confirming that E10 and E32 are not involved in any electrostatic interaction that controls the conformational flexibility of the peptide. Thus, only the E23 mutation is directly involved in causing electrostatically tunable conformational rigidity at the CTD.

Ensemble CD Measurements Reveal that All Three Phosphorylation Mimicking Mutations are Required for an Enhancement in the Secondary Structure of the Peptide. Ensemble circular dichroism (CD) spectroscopy is utilized to compare the secondary structures of the peptides, and the results are depicted in Figure 4. It is important to note that the peptides are short and exhibit a weak CD signal as they do not have the extensive α-helical or β-sheet structure characteristic of a protein with a well-defined secondary structure. However, the CD does indicate of the relative stability of the peptides. The E10E23E32 peptide shows a stronger CD signal compared to the native peptide, as reported

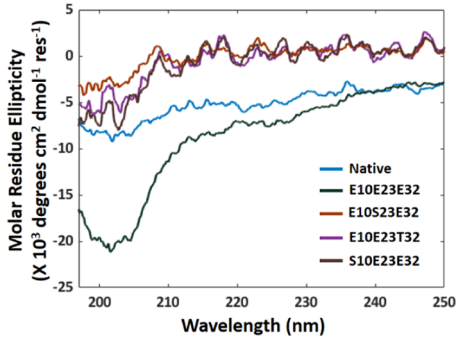

Figure 4. All three mutations together enhance the secondary structure of the peptide. CD spectra of the native (blue), the E10E23E32 peptide (dark green), the E10S23E32 peptide (light brown), the E10E23T32 peptide (purple), and the S10E23E32 peptide (dark brown), under standard buffer (1×) condition, are shown. Only when all three mutations are present, a stronger random-coiled secondary structure is observed, as compared to the native peptide and the mutants containing only two mutations.

previously,[23] indicating that phosphomimicry enhances the random-coil nature of the secondary structure of the native peptide. CD signal intensities exhibited by all three mutants are still random-coil like but are less ordered relative to both the native and the E10E23E32 peptides. This observation indicates that all three mutations are necessary for a stronger random-coiled structure and supports the first step of our proposed mechanism that phosphomimicry at all three sites together leads to a substantial change in the secondary structure.

At a high ionic strength, the E10E23T32 and the S10E23E32 peptides retain their secondary structure (Figure S5), even though they lose their conformational rigidity, as shown by the smFRET data above. Such contradictory

DOI: 10.1021/acsomega.9b01384
ACS Omega 2019, 4, 14211−14218

conformational behavior indicates that high ionic strength, without affecting the peptide structure, shields the electrostatic interaction, which stabilizes the peptide in a rigid conformation. Thus, it validates the second step of the proposed mechanism that the secondary structure gained in the first step is stabilized through an electrostatic interaction, involving E23, resulting in the conformational rigidity. Furthermore, combined with the smFRET results, it is evident that even though the E23 mutation along with either E10 or E32 does not enhance the secondary structure, yet, those weakly random-coiled structures get stabilized by the electrostatic interaction. Additionally, the E10S23E32 peptide shows a weaker CD signal as compared to the E10E23T32 and the S10E23E32 peptides, indicating lesser random-coil nature in the absence of E23. Thus, E23 is not only involved in an electrostatic tertiary stabilization of the peptide but also plays an important role in strengthening the secondary structure of the peptide.

CONCLUSIONS

Our study provides direct experimental support to a previously proposed mechanism[23] for the phosphorylation occurring at the CTD of the AMPA receptors. With the stepwise mutation strategy, we have demonstrated that phosphorylation at all of the three sites, namely, S818 (E10), S831 (E23), and T840 (E32), is necessary for introducing a stronger random-coiled nature to the otherwise disordered secondary structure of the native sequence. The secondary structure is further stabilized by a possible tertiary structure formation through electrostatic interaction involving only the phosphomutated S831 (E23) site. This two-step mechanism provides a concrete explanation for the electrostatically tunable conformational rigidity, introduced by phosphorylation mimicking mutations at the above-mentioned phosphorylation targets. We speculate that the conformational rigidity caused by phosphorylation in the CTD causes the ion channel to stay open for longer, which enhances the flow of the ion. The build-up of ion inside the membrane shields the electrostatic interaction and brings back the conformational flexibility leading to desensitization of the ion channels.

Furthermore, our study distinguishes the role of phosphomutated S831 (E23) specifically as the primary contributor toward the conformational rigidity possibly through the formation of the salt bridge with nearby positively charged residues [Arginines (R7, R12, R29) and Lysines (K5, K14)]. Further studies on the single mutated S831 (E23) peptide and substituted peptides (positively charged residues substituted by neutral amino acids) are required for a comprehensive understanding of the role of S831 (E23) mutation and the nature of the salt bridge. Our findings further need to be correlated with similar experimental investigations performed under a more physiologically relevant condition. For example, a detailed study on the CTD within the full-length AMPA receptor will elucidate how the conformation of the rest of the protein and the conformational changes induced by phosphorylation affect each other. Also, the CTD mutants are dynamic; computational structure prediction algorithms fail to identify stable conformations.[23] We think such dynamic yet functional peptide structures offer a challenge for the development of future theory.

MATERIALS AND METHODS

Peptide Sequences and Labeling. Peptides were ordered from Peptide 2.0 Inc. The native unphosphorylated peptide has a primary sequence of EFCYKSRSESKRMKGFSLIPQQSINEAIRTSTLC (native peptide).[23] The underlined S indicates C17S point mutation, which is a common strategy to prevent unwanted Cysteine labeling by fluorophores.[23,39,44] One Cysteine (C34) was also introduced to house another label at the C-terminal end of the sequence. Thus, specific labeling at both ends of the peptide construct was achieved. To mimic phosphorylation, S10E, S23E, and T32E mutations were introduced, corresponding to the phosphorylations at S818, S831, and T840 making the sequence EFCYKSRSEEKRMKGFSLIPQQEINEAIRTSELC (E10E23E32 peptide). Three other mutant peptides were also studied, in each of which, one of the mutations was turned off by leaving the native amino acid unmutated. The sequences of these mutants are EFCYKSRSEEKRMKGFSLIPQQSINEAIRTSELC (E10S23E32), EFCYKSRSEEKRMKGFSLIPQQEINEAIRTSTLC (E10E23T32), and EFCYKSRSESKRMKGFSLIPQQEINEAIRTSELC (S10E23E32). All of the peptides also had a biotin tag at the N-terminus to allow immobilization through biotin−streptavidin interaction. The peptides were dissolved in standard 1× phosphate-buffered saline (Santacruz Biotechnologies; 137 mM NaCl, 2.7 mM KCl, 10 mM Na_2HPO_4, and 1.8 mM KH_2PO_4) and stored as 150 μM stock aliquots at −20 °C.

To label the peptides with a pair of donor−acceptor fluorophores, Alexa 555 maleimide ester (Life technologies) and Alexa 647 maleimide ester (Life technologies) were added to a 2−3 μM solution of the peptides at a 1:1:4 concentration ratio of the peptides:Alexa 555(donor):Alexa 647(acceptor). C3 and C34, the only Cysteine residues in the peptides ensured site-specific labeling with the donor−acceptor fluorophores through the cysteine−maleimide interaction. The labeled sample was left to equilibrate at 4−6 °C for ∼1 h. The resulting solution was then diluted to 2−3 nM with respect to the concentration of the peptide, for immobilization.

Sample Chamber Preparation. A detailed protocol for the preparation of the sample can be found in previous publications.[23,27,45] In brief, glass coverslips (no. 1, 22 × 22 mm^2, Fischer Scientific) were sonicated in acetone, soapy water, and Millipore water and then treated for 90 s in the TL1 solution composed of 4% (v/v) H_2O_2 (Fisher Scientific, Radnor, PA) and 13% (v/v) NH_4OH at 75 °C. The coverslips were then washed with Millipore water and dried with nitrogen. Next, they were cleaned for 2 min under O_2 plasma (PDC-32G, Harrick Plasma). Plasma-cleaned coverslips were then treated with Vectabond−acetone solution (2% vol/vol, Vector Laboratories, Burlingame, CA) for aminosilanization. PEG-BiotinPEG solution containing 5 kDa mPEG succinimidyl carbonate (25% w/w, Laysan Bio, in molecular biology grade (MB) water, GE Lifesciences), 5 kDa biotin terminated PEG (2.5% w/w in MB water, NOF corp.), and sodium bicarbonate (Sigma-Aldrich) was prepared. A silicone template (43018 M, Grace BioLabs) was placed on top of the coverslip to add the PEG-BioPEG solution to a specific area on the coverslip. The PEG-coated coverslips were left to incubate in a dark and humid environment overnight. Afterward, excess PEG-BioPEG solution was rinsed off with MB water and dried with Nitrogen gas. HybriWell custom chambers (43018 C, Grace BioLabs) fitted with two custom silicone ports (460003,

DOI: 10.1021/acsomega.9b01384
ACS Omega 2019, 4, 14211−14218

Grace BioLabs) were placed on top of the coverslips to create a sealed chamber and to allow the flow of the solution through it.

Protein Immobilization. A 0.2 mg/mL of the solution of streptavidin prepared in 1× PBS buffer was flowed into the sealed chamber. After 10 min, 2−3 nM of the labeled peptide solution was added, followed by equilibration for 20 min and a subsequent wash with a copious amount of the buffer solution, to wash off unbound peptides and free dyes. For higher salt concentration experiments, PBS buffer solutions with corresponding salt concentrations (2×: [NaCl] = 274 mM, [KCl] = 5.4 mM; 5×: [NaCl] = 685 mM, [KCl] = 13.5 mM) were added, and the chambers were left to equilibrate for 10−15 min prior to acquisitions.

smFRET Data Acquisition. smFRET acquisition was performed using a home-built confocal microscope described in details previously.[27,45] Briefly, the excitation light was focused onto the sample via an oil immersion objective (100 × 1.3 NA, Carl Zeiss) with a power density of ∼50 μW/cm^2. The emitted light collected with the same objective was split by a 640 nm high-pass dichroic mirror, (640 DCXR, Chroma Technology) to collect the donor and acceptor signals at two avalanche photodiodes (SPCM-AQR-15, Perkin Elmer), separately and simultaneously. Band-pass filters (NHPF-532.0, Kaiser Optical Systems) were used to exclude the excitation light, tuning the light to the emission ranges for donor and acceptor. Using a closed-loop x-y-z piezo stage (P-517.3CL, Physik Instrumente), multiple 10 μm areas were scanned and corresponding images were acquired, with both 532 nm CW laser (Compass 315M-100SL, Coherent) and 637 nm laser (OBIS-FP 637 LX, Coherent) to determine the locations of peptides exhibiting FRET. Representative scan images are presented in Figure S6 in the Supporting Information. Peptide molecules were then selected one by one, excited at 532 nm, and donor−acceptor emissions were collected for each molecule. All acquisitions were done in the presence of an oxygen scavenging and photostabilizing buffer (ROXS) composed of 1 mM methyl viologen, 1 mM ascorbic acid, 1% w/w glucose oxidase, 0.1% v/v catalase, and 33% w/w D-(+)-glucose (all from Sigma-Aldrich) in 1× PBS buffer. For higher salt concentration experiments, ROXS was prepared in the PBS buffer containing corresponding salt concentrations.

Data Analysis. Data processing and analysis were performed in MATLAB (R2018a, MathWorks). Donor and acceptor fluorescence emission signals were collected from each single-peptide molecules.[46,47] Apparent smFRET efficiency trajectories, $E_A(t)$, were calculated from the background and cross-talk-corrected donor and acceptor fluorescence intensities ($I_D(t)$ and $I_A(t)$ respectively) using eq 1, as given below.[48,49] Apparent FRET efficiency, $E_A(t)$, is related to the actual FRET efficiency, $E_{FRET}(t)$ by eq 2, where Φ_D and Φ_A are quantum efficiencies of the donor and acceptor fluorophores, respectively, and η_D and η_A are the detector quantum efficiencies. For our experimental setup, $(\Phi_D\Phi_A/\eta_D\eta_A) \sim 1$, thereby making $E_A(t) \sim E_{FRET}(t)$.[45,49,50] Each apparent smFRET efficiency trajectory ($E_A(t)$) was processed using a wavelet denoising algorithm[46,47] and was subjected to various checks to remove trajectories exhibiting multistep photobleaching or an abnormally low signal to noise ratio. Trajectories not exhibiting anticorrelation between the donor and acceptor intensities were also discarded. The donor−acceptor distances (r) were calculated from the apparent FRET efficiencies ($E_A(t)$) using eq 3, where R_0 (= 51 Å) is the Förster radius for the donor−acceptor fluorophores (Alexa 555 and Alexa 647, Molecular Probes).[45]

$$E_A(t) = \frac{I_A(t)}{I_A(t) + I_D(t)} \quad (1)$$

$$E_{FRET}(t) = \frac{I_A(t)}{I_A(t) + I_D(t)\frac{\Phi_A\eta_A}{\Phi_D\eta_D}} \quad (2)$$

$$E_A = \frac{R_0^6}{R_0^6 + r^6} \quad (3)$$

Finally, all single-molecule E_A trajectories (for a particular mutant) are combined to generate the distribution of FRET efficiency values explored by the mutant at each time point of those single-molecule trajectories.

Circular Dichroism (CD) Spectroscopy. CD spectra for all peptides were acquired using a Jasco J-810 spectropolarimeter. Native, E10E23E32 and E10S23E32 peptide solutions were prepared in the PBS buffer at 75 μM concentration. E10E23T32 and S10E23E32 were prepared at 50 μM concentration. All five peptides were prepared in high salt concentration buffer solutions as well. After preparation, all of the peptide solutions were allowed to equilibrate for 15 min at room temperature prior to data collection. Measurements were conducted at room temperature, from wavelengths of 180−250 nm, with a scan speed of 20 nm/min, in a 0.01 cm quartz cuvette, using 20 μL of each solution. Data obtained in millidegrees were averaged over 5 accumulations with a data pitch of 0.1 nm. Data in millidegrees were then converted to molar residue ellipticity ($[\theta]$) using the equation $[\theta] = \frac{\theta}{l \times N \times c \times 10}$ where θ is ellipticity in degrees reported by the instrument, l is the pathlength of the cuvette in cm, N is the number of residues in the protein, and c is the concentration of the protein in g/cm^3. CD spectra were plotted from 195 to 250 nm to avoid the noise caused by the presence of salt below 195 nm.

■ ASSOCIATED CONTENT

Supporting Information

The Supporting Information is available free of charge on the ACS Publications website at DOI: 10.1021/acsomega.9b01384.

Example smFRET data corresponding to NMDA receptor protein, vbFRET analysis for all three mutants, distribution of SD of smFRET efficiency for each mutant, smFRET efficiency and CV analysis for the native and the E10S23E32 peptide under varying salt concentration, CD spectra for all of the mutants under varying salt concentration, representative scan images, representative smFRET trajectories, relative occurrences of different FRET efficiency ranges for each mutant and statistics of smFRET measurements (PDF)

■ AUTHOR INFORMATION

Corresponding Author

*E-mail: cflandes@rice.edu. Tel: (713) 348-4232.

ORCID

Sudeshna Chatterjee: 0000-0001-8733-0587

Chayan Dutta: 0000-0003-4839-2245

Christy F. Landes: 0000-0003-4163-6497

DOI: 10.1021/acsomega.9b01384
ACS Omega 2019, 4, 14211−14218

Notes

The authors declare no competing financial interest.

■ ACKNOWLEDGMENTS

This work is supported by the Welch Foundation (grant no. C-1787). C.D. thanks the National Science Foundation (grant no. CHE-1808382) for funding. The authors thank Prof. Vasanthi Jayaraman and her group at UTHSC for the collaboration on the NMDA receptor protein study shown in the Supporting Information. The authors thank all of the members of the Landes research group, Prof. Stephan Link and his research group for helpful discussions.

■ REFERENCES

(1) Watkins, J. C.; Jane, D. E. The glutamate story. *Br. J. Pharmacol.* **2006**, *147*, S100−S108.
(2) Traynelis, S. F.; Wollmuth, L. P.; McBain, C. J.; Menniti, F. S.; Vance, K. M.; Ogden, K. K.; Hansen, K. B.; Yuan, H.; Myers, S. J.; Dingledine, R. Glutamate receptor ion channels: Structure, regulation, and function. *Pharmacol. Rev.* **2010**, *62*, 405−496.
(3) Prieto, M. L.; Wollmuth, L. P. Gating modes in AMPA receptors. *J. Neurosci.* **2010**, *30*, 4449.
(4) Shepherd, J. D.; Huganir, R. L. The cell biology of synaptic plasticity: AMPA receptor trafficking. *Annu. Rev. Cell Dev. Biol.* **2007**, *23*, 613−643.
(5) Madden, D. R. The structure and function of glutamate receptor ion channels. *Nat. Rev. Neurosci.* **2002**, *3*, 91−101.
(6) Boehm, J.; Malinow, R. AMPA receptor phosphorylation during synaptic plasticity. *Biochem. Soc. Trans.* **2005**, *33*, 1354.
(7) Granger, A. J.; Shi, Y.; Lu, W.; Cerpas, M.; Nicoll, R. A. LTP requires a reserve pool of glutamate receptors independent of subunit type. *Nature* **2013**, *493*, 495−500.
(8) Lee, H.-K.; Takamiya, K.; He, K.; Song, L.; Huganir, R. L. Specific roles of AMPA receptor subunit GluR1 (GluA1) phosphorylation sites in regulating synaptic plasticity in the CA1 region of hippocampus. *J. Neurophysiol.* **2010**, *103*, 479.
(9) Malinow, R. LTP: Desperately seeking resolution. *Science* **1994**, *266*, 1195.
(10) Lee, H.-K.; Takamiya, K.; Han, J.-S.; Man, H.; Kim, C.-H.; Rumbaugh, G.; Yu, S.; Ding, L.; He, C.; Petralia, R. S.; Wenthold, R. J.; Gallagher, M.; Huganir, R. L. Phosphorylation of the AMPA receptor GluR1 subunit is required for synaptic plasticity and retention of spatial memory. *Cell* **2003**, *112*, 631−643.
(11) Barria, A.; Muller, D.; Derkach, V.; Griffith, L. C.; Soderling, T. R. Regulatory phosphorylation of AMPA-type glutamate receptors by CaM-KII during long-term potentiation. *Science* **1997**, *276*, 2042.
(12) Lin, D.-T.; Makino, Y.; Sharma, K.; Hayashi, T.; Neve, R.; Takamiya, K.; Huganir, R. L. Regulation of AMPA receptor extrasynaptic insertion by 4.1N, phosphorylation and palmitoylation. *Nat. Neurosci.* **2009**, *12*, 879−887.
(13) Blackstone, C.; Murphy, T. H.; Moss, S. J.; Baraban, J. M.; Huganir, R. L. Cyclic AMP and synaptic activity-dependent phosphorylation of AMPA- preferring glutamate receptors. *J. Neurosci.* **1994**, *14*, 7585.
(14) Boehm, J.; Kang, M.-G.; Johnson, R. C.; Esteban, J.; Huganir, R. L.; Malinow, R. Synaptic incorporation of AMPA receptors during LTP is controlled by a PKC phosphorylation site on GluR1. *Neuron* **2006**, *51*, 213−225.
(15) Chang, P. K. Y.; Verbich, D.; McKinney, R. A. AMPA receptors as drug targets in neurological disease − advantages, caveats, and future outlook. *Eur. J. Neurosci.* **2012**, *35*, 1908−1916.
(16) Johnson, K. A.; Conn, P. J.; Niswender, C. M. Glutamate receptors as therapeutic targets for parkinson's disease. *CNS Neurol. Disord.: Drug Targets* **2009**, *8*, 475−491.
(17) Lee, K.; Goodman, L.; Fourie, C.; Schenk, S.; Leitch, B.; Montgomery, J. M. Chapter six - AMPA receptors as therapeutic targets for neurological disorders. In *Advances in Protein Chemistry and Structural Biology*; Donev, R., Ed.; Academic Press, 2016; Vol. *103*, pp 203−261.
(18) White, S. L.; Ortinski, P. I.; Friedman, S. H.; Zhang, L.; Neve, R. L.; Kalb, R. G.; Schmidt, H. D.; Pierce, R. C. A critical role for the GluA1 accessory protein, SAP97, in cocaine seeking. *Neuropsychopharmacology* **2016**, *41*, 736−750.
(19) Sobolevsky, A. I.; Rosconi, M. P.; Gouaux, E. X-ray structure, symmetry and mechanism of an AMPA-subtype glutamate receptor. *Nature* **2009**, *462*, 745−756.
(20) Jenkins, M. A.; Traynelis, S. F. PKC phosphorylates GluA1-Ser831 to enhance AMPA receptor conductance. *Channels* **2012**, *6*, 60−64.
(21) Jenkins, M. A.; Wells, G.; Bachman, J.; Snyder, J. P.; Jenkins, A.; Huganir, R. L.; Oswald, R. E.; Traynelis, S. F. Regulation of GluA1 α-Amino-3-hydroxy-5-methyl-4-isoxazolepropionic acid receptor function by protein kinase c at Serine-818 and Threonine-840. *Mol. Pharmacol.* **2014**, *85*, 618.
(22) Kristensen, A. S.; Jenkins, M. A.; Banke, T. G.; Schousboe, A.; Makino, Y.; Johnson, R. C.; Huganir, R.; Traynelis, S. F. Mechanism of Ca^{2+}/calmodulin-dependent kinase II regulation of AMPA receptor gating. *Nat. Neurosci.* **2011**, *14*, 727−735.
(23) Chatterjee, S.; Ade, C.; Nurik, C. E.; Carrejo, N. C.; Dutta, C.; Jayaraman, V.; Landes, C. F. Phosphorylation induces conformational rigidity at the c-terminal domain of AMPA receptors. *J. Phys. Chem. B* **2019**, *123*, 130−137.
(24) Tavalin, S. J. AKAP79 selectively enhances protein kinase c regulation of GluR1 at a Ca2+-calmodulin-dependent protein kinase II/protein kinase c site. *J. Biol. Chem.* **2008**, *283*, 11445−11452.
(25) Derkach, V.; Barria, A.; Soderling, T. R. Ca^{2+}/calmodulin-kinase II enhances channel conductance of α-Amino-3-hydroxy-5-methyl-4-isoxazolepropionate type glutamate receptors. *Proc. Natl. Acad. Sci. U.S.A.* **1999**, *96*, 3269−3274.
(26) Dolino, D. M.; Rezaei Adariani, S.; Shaikh, S. A.; Jayaraman, V.; Sanabria, H. Conformational selection and submillisecond dynamics of the ligand-binding domain of the N-methyl-D-Aspartate receptor. *J. Biol. Chem.* **2016**, 16175−16185.
(27) Cooper, D. R.; Dolino, D. M.; Jaurich, H.; Shuang, B.; Ramaswamy, S.; Nurik, C. E.; Chen, J.; Jayaraman, V.; Landes, C. F. Conformational transitions in the glycine-bound GluN1 NMDA receptor LBD via single-molecule FRET. *Biophys. J.* **2015**, *109*, 66−75.
(28) Dolino, D. M.; Cooper, D.; Ramaswamy, S.; Jaurich, H.; Landes, C. F.; Jayaraman, V. Structural dynamics of the glycine-binding domain of the N-methyl-D-aspartate receptor. *J. Biol. Chem.* **2015**, *290*, 797−804.
(29) He, Y.; Lu, M.; Cao, J.; Lu, H. P. Manipulating protein conformations by single-molecule AFM-FRET nanoscopy. *ACS Nano* **2012**, *6*, 1221−1229.
(30) Roy, R.; Hohng, S.; Ha, T. A practical guide to single-molecule FRET. *Nat. Methods* **2008**, *5*, 507−516.
(31) Sasmal, D. K.; Yadav, R.; Lu, H. P. Single-molecule patch-clamp FRET anisotropy microscopy studies of NMDA receptor ion channel activation and deactivation under agonist ligand binding in living cells. *J. Am. Chem. Soc.* **2016**, *138*, 8789−8801.
(32) Stultz, C. M.; Levin, A. D.; Edelman, E. R. Phosphorylation-induced conformational changes in a mitogen-activated protein kinase substrate: Implications for tyrosine hydroxylase activation. *J. Biol. Chem.* **2002**, *277*, 47653−47661.
(33) Karam, P.; Powdrill, M. H.; Liu, H.-W.; Vasquez, C.; Mah, W.; Bernatchez, J.; Götte, M.; Cosa, G. Dynamics of hepatitis c virus (HCV) RNA-dependent RNA polymerase NS5B in complex with RNA. *J. Biol. Chem.* **2014**, *289*, 14399−14411.
(34) Holley, S. M.; Ahmed, A. H.; Srinivasan, J.; Murthy, S. E.; Weiland, G. A.; Oswald, R. E.; Nowak, L. M. The loss of an electrostatic contact unique to AMPA receptor ligand binding domain 2 slows channel activation. *Biochemistry* **2012**, *51*, 4015−4027.
(35) Li, J.; Bigelow, D. J.; Squier, T. C. Phosphorylation by cAMP-dependent protein kinase modulates the structural coupling between

DOI: 10.1021/acsomega.9b01384
ACS Omega 2019, 4, 14211−14218

the transmembrane and cytosolic domains of phospholamban. *Biochemistry* **2003**, *42*, 10674−10682.
(36) Miranda, F. F.; Thórólfsson, M.; Teigen, K.; Sanchez-Ruiz, J. M.; Martínez, A. Structural and stability effects of phosphorylation: Localized structural changes in phenylalanine hydroxylase. *Protein Sci.* **2004**, *13*, 1219−1226.
(37) Bhattarai, N.; Gerstman, B. S.; Chapagain, P. P. Role of k-loop cysteine residues in the marburg virus protein VP24−human Keap1 complex. *ACS Omega* **2018**, *3*, 18639−18645.
(38) Kannan, S.; Pradhan, M. R.; Cherian, J.; Joseph, T. L.; Poh, Z. Y.; Hai Yan, Y.; Melvyn, H.; Boping, L.; Jeffrey, H.; Nacro, K.; Verma, C. S. Small molecules targeting the inactive form of the Mnk1/2 kinases. *ACS Omega* **2017**, *2*, 7881−7891.
(39) Dolino, D. M.; Chatterjee, S.; MacLean, D. M.; Flatebo, C.; Bishop, L. D. C.; Shaikh, S. A.; Landes, C. F.; Jayaraman, V. The structure−energy landscape of NMDA receptor gating. *Nat. Chem. Biol.* **2017**, *13*, 1232.
(40) Karakas, E.; Furukawa, H. Crystal structure of a heterotetrameric NMDA receptor ion channel. *Science* **2014**, *344*, 992.
(41) Bronson, J. E.; Fei, J.; Hofman, J. M.; Gonzalez, R. L.; Wiggins, C. H. Learning rates and states from biophysical time series: A bayesian approach to model selection and single-molecule FRET data. *Biophys. J.* **2009**, *97*, 3196−3205.
(42) Thévenet, P.; Shen, Y.; Maupetit, J.; Guyon, F.; Derreumaux, P.; Tufféry, P. PEP-FOLD: An updated de novo structure prediction server for both linear and disulfide bonded cyclic peptides. *Nucleic Acids Res.* **2012**, *40*, W288−W293.
(43) Jayaram, B.; Bhushan, K.; Shenoy, S. R.; Narang, P.; Bose, S.; Agrawal, P.; Sahu, D.; Pandey, V. Bhageerath: An energy based web enabled computer software suite for limiting the search space of tertiary structures of small globular proteins. *Nucleic Acids Res.* **2006**, *34*, 6195−6204.
(44) Ramaswamy, S.; Cooper, D.; Poddar, N.; MacLean, D. M.; Rambhadran, A.; Taylor, J. N.; Uhm, H.; Landes, C. F.; Jayaraman, V. Role of conformational dynamics in α-Amino-3-hydroxy-5-methyl-isoxazole-4-propionic acid (AMPA) receptor partial agonism. *J. Biol. Chem.* **2012**, *287*, 43557−43564.
(45) Landes, C. F.; Rambhadran, A.; Taylor, J. N.; Salatan, F.; Jayaraman, V. Structural landscape of isolated agonist-binding domains from single AMPA receptors. *Nat. Chem. Biol.* **2011**, *7*, 168−173.
(46) Taylor, J. N.; Landes, C. F. Improved resolution of complex single-molecule FRET systems via wavelet shrinkage. *J. Phys. Chem. B* **2011**, *115*, 1105−1114.
(47) Taylor, J. N.; Makarov, D. E.; Landes, C. F. Denoising single-molecule FRET trajectories with wavelets and bayesian inference. *Biophys. J.* **2010**, *98*, 164−173.
(48) Cosa, G.; Harbron, E. J.; Zeng, Y.; Liu, H.-W.; O'Connor, D. B.; Eta-Hosokawa, C.; Musier-Forsyth, K.; Barbara, P. F. Secondary structure and secondary structure dynamics of DNA hairpins complexed with HIV-1 NC Protein. *Biophys. J.* **2004**, *87*, 2759−2767.
(49) Landes, C. F.; Zeng, Y.; Liu, H.-W.; Musier-Forsyth, K.; Barbara, P. F. Single-molecule study of the inhibition of HIV-1 transactivation response region DNA/DNA annealing by arginina-mide. *J. Am. Chem. Soc.* **2007**, *129*, 10181−10188.
(50) Hellenkamp, B.; Schmid, S.; Doroshenko, O.; Opanasyuk, O.; Kühnemuth, R.; Rezaei Adariani, S.; Ambrose, B.; Aznauryan, M.; Barth, A.; Birkedal, V.; Bowen, M. E.; Chen, H.; Cordes, T.; Eilert, T.; Fijen, C.; Gebhardt, C.; Götz, M.; Gouridis, G.; Gratton, E.; Ha, T.; Hao, P.; Hanke, C. A.; Hartmann, A.; Hendrix, J.; Hildebrandt, L. L.; Hirschfeld, V.; Hohlbein, J.; Hua, B.; Hübner, C. G.; Kallis, E.; Kapanidis, A. N.; Kim, J.-Y.; Krainer, G.; Lamb, D. C.; Lee, N. K.; Lemke, E. A.; Levesque, B.; Levitus, M.; McCann, J. J.; Naredi-Rainer, N.; Nettels, D.; Ngo, T.; Qiu, R.; Robb, N. C.; Röcker, C.; Sanabria, H.; Schlierf, M.; Schröder, T.; Schuler, B.; Seidel, H.; Streit, L.; Thurn, J.; Tinnefeld, P.; Tyagi, S.; Vandenberk, N.; Vera, A. M.; Weninger, K. R.; Wünsch, B.; Yanez-Orozco, I. S.; Michaelis, J.; Seidel, C. A. M.; Craggs, T. D.; Hugel, T. Precision and accuracy of single-molecule FRET measurements—a multi-laboratory benchmark study. *Nat. Methods* **2018**, *15*, 669−676.

DOI: 10.1021/acsomega.9b01384
ACS Omega 2019, 4, 14211−14218